Unsubstituted Cyclidenes—A Novel Family of Lacunar Dioxygen Carriers with Enhanced Stability toward Autoxidation: Synthesis, Characterization, and a Representative X-ray Structure

A. G. Kolchinski,[†] B. Korybut-Daszkiewicz,[†,§] E. V. Rybak-Akimova,[†] D. H. Busch,*[,†] N. W. Alcock,[‡] and H. J. Clase[‡]

Contribution from the Department of Chemistry, University of Kansas, Lawrence, Kansas 66045, and Department of Chemistry, University of Warwick, Coventry CV4 7AL, United Kingdom

Received July 16, 1996[⊗]

Abstract: A major advance has been made in the incremental molecular design of long-lived cobalt(II) dioxygen carriers. Preceding mechanistic studies revealed that ionizable methyl groups trigger the autoxidation of the O_2 adduct of the cobalt(II) cyclidene. Two members of a new family of unsubstituted (no methyl groups) lacunar cyclidene dioxygen carriers have been prepared in an eight-step synthesis, and a complex with a hexamethylene bridge has been structurally characterized. In contrast to previously studied cyclidenes, these materials bear no substituents on the chelated macrocyclic platform. As anticipated, the rates of autoxidation of these unsubstituted cyclidene complexes were found to be 5−8 times slower than those for the most stable previously known cyclidene derivatives. Because of the absence of Me−Me vicinal repulsion, the C6 bridge assumes a zig-zag conformation directly across the cavity. The accompanying, relatively low, dioxygen affinity is explained on the basis of electronic and steric factors. The rates of dioxygen binding to these newly prepared cobalt(II) unsubstituted cyclidenes are fast and approximately equal to the corresponding values for their Me-substituted analogs. Consequently, differences in dissociation rates are responsible for the differences in O_2 affinities. This is a clear example of an unusual steric effect for O_2 adducts.

Introduction

The preparation and investigation of synthetic reversible dioxygen carriers has attracted substantial interest in recent years,[1] and their physico-chemical properties are sufficiently favorable that they have been considered for applications in the air separation and other industries.[1ac] Such exploitation has been hampered by an intrinsic feature of synthetic, as well as natural, dioxygen carriers, their irreversible oxidation by dioxygen (autoxidation). Even the most successful biological dioxygen carrier, hemoglobin, undergoes 1.5−3% autoxidation per day (human Hb).[2] The autoxidation process determines the potential service lifetime of synthetic dioxygen carriers, and, therefore, limits their utility. While those concerned with applications have turned to other technologies,[1c] we see in this the great need to understand the mechanisms of autoxidation and to direct that knowledge toward the molecular design and synthesis of new dioxygen carriers with enhanced functional lifetimes. In circumstances of this kind, an ultimate test of mechanism may be found in the guidance it provides in the design of improved molecules. Iterative molecular design is a natural consequence of this perspective because elimination of one autoxidation mechanism may reveal an underlying mechanism that, while slower, may still operate at troublesome rates. The broad realization that formation of peroxo-bridged intermediates is key to a dominant mechanism of autoxidation[3] for many familar transition metal dioxygen carriers, especially those of iron(II), led to the picket fence porphyrins, the lacunar complexes described here, and other innovative molecular designs.[4,1b] These advances in structure eliminated the peroxo-bridged mechanism and were followed by studies that revealed new, albeit much slower, autoxidation mechanisms.[5] The mechanisms in the case of the iron(II) complexes have been discussed elsewhere;[1b,3c] here we will treat only those associated with lacunar cobalt(II) complexes, with focus on those of the cyclidene ligands of the family used in the present studies.

The cobalt(II) and iron(II) cyclidene dioxygen carriers (Figure 1) are among the most successful classes of non-porphyrin dioxygen carriers.[1b] They include complexes with a wide range of dioxygen affinities, solubilities, and stabilities toward autoxidation. Most of them contain a hydrophobic cavity (created

[†] University of Kansas.
[‡] University of Warwick.
[§] Institute of Organic Chemistry, Polish Academy of Sciences, O1-224 Warsaw, Poland.
[⊗] Abstract published in *Advance ACS Abstracts,* April 15, 1997.

(1) (a) Haggin, J. *Chem. Eng. News* **1996**, Feb. 5, 35. (b) Busch, D. H.; Alcock, N. W. *Chem. Rev.* **1994**, *94*, 585. (c) Li, G. Q.; Govind, R. *Ind. Eng. Chem. Res*. **1994**, *33*, 755. (d) Martell, A. E.; Motekaitis, R. J.; Rockcliffe, D.; Menif, R.; Ngwenya, P. M. *Pure Appl. Chem*. **1994**, *66*, 859. (e) Traylor, T. G.; Traylor, P. S. *Annual Rev. Biophys. Bioeng*. **1982**, *11*, 105. (f) Collman, J. P., Halpert, T. R.; Suslick, K. S. In *Metal Ion Activation of Dioxygen*; Spiro, T. G., Ed.; Wiley & Sons: New York, 1980. (g) Niederhoffer, E. C.; Timmons, J. H.; Martell, A. E. *Chem. Rev.* **1984**, *84*, 137. (h) Smith, T. D.; Pilbrow, J. T. *Coord. Chem. Rev.* **1981**, *39*, 295. (i) Jones, R. D.; Summerville, D. A.; Basolo, F. *Chem. Rev.* **1979**, *79*, 139. (j) McLendon, G.; Martell, A. E. *Coord. Chem. Rev*. **1976**, *19*, 1. (k) Vaska, L. *Acc. Chem. Res*. **1976**, *9*, 175.
(2) Jaffe, E. R.; Neuman, G. *Nature* **1964**, *202*, 607.
(3) (a) Hammond, G. S.; Wu, C.-H. *Adv. Chem. Series*. **1968**, *77*, 186. (b) Alben, J. O.; Fuchsman, W. H.; Beaudreau, C. A.; Caughey, W. S. *Biochemistry* **1968**, *7*, 624. (c) Warburton, P. R.; Busch, D. H. Dynamics of IronII and CobaltII Dioxygen Carriers. In *Perspectives on Bioinorganic Chemistry*; Hay, R. W., Dilworth, J. R., Nolan, K. B., Eds.; JAI Press Ltd.: London, 1993; Vol. 2, pp 1−79.
(4) (a) Collman, J. P.; Gagnè, R. R.; Reed, C. A. *J. Am. Chem. Soc.* **1974**, *96*, 6522. (b) Collman, J. P.; Elliott, C. M.; Halbert, T. R.; Tovrog, B. S. *Proc. Natl. Acad. Sci. U.S.A.* **1977**, *74*, 18. (c) Collman, J. P.; Brauman, J. I.; Collins, T. J.; Iverson, B. L.; Sessler, J. L. *J. Am. Chem. Soc.* **1981**, *103*, 2450. (d) Momenteau, M.; Reed, C. A. *Chem. Rev.* **1994**, *94*, 659.
(5) (a) Wallace, W. J.; Maxwell, J. C.; Caughey, W. S. *Biochem. Biophys. Res. Commun*. **1974**, *57*, *4*, 1104. (b) Shikama, K. *Coord. Chem. Rev.* **1988**, *83*, 73−91. (c) Wallace, W. J.; Houtchens, R. A.; Maxwell, J. C.; Caughey, W. S. *J. Biol. Chem*. **1982**, *257*, 4966.

S0002-7863(96)02447-X CCC: $14.00

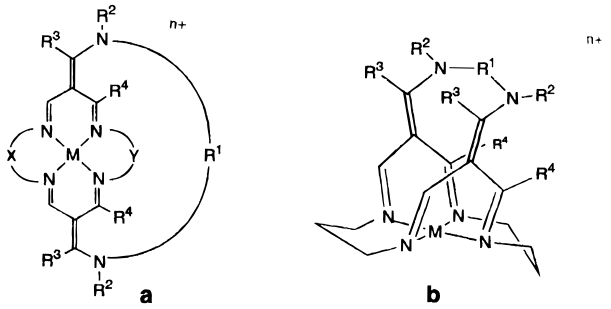

Figure 1. Planar (a) and three-dimensional (b) representations of cyclidene complexes; denoted below as M($R^1R^2R^3R^4$cyclidene), where M = Ni or Co.

by a bridging group) into which dioxygen (or some other small ligand) may enter. The opposite, and external, axial site is occupied by an auxiliary nitrogenous base, which is usually present in the reaction mixture in large excess. The general cyclidene structure (Figure 1) allows extensive modification by changing substituents R^2 and R^3 and/or the linking groups R^1, X, and Y. For the compounds of major interest to this paper, the chelating groups X and Y remain unchanged (X = Y = $(CH_2)_3$), while bridge R^1 is always $(CH_2)_n$ (or simply Cn in formulas). This paper addresses R^4, which has hitherto always been CH_3, but is H in the new compounds reported here. Cyclidene formulas will be presented in a simplified manner as ($CnR^2R^3R^4$Cyc), where *n* is the number of methylene groups in the bridge R^1, and R^2, R^3, and R^4 are the substituents.

Earlier studies have provided vital mechanistic insight into the autoxidation of cobalt(II) cyclidenes.[6] A well demonstrated and critical feature of the proposed mechanism is the deprotonation of the dioxygenated cobalt(II) complex to produce a conjugate base derivative that is vulnerable to irreversible oxidation of the ligand. The generality of this mechanistic feature had long been apparent. When R^2 is hydrogen, the relatively acidic N-H proton leads to relatively rapid autoxidation, and most of the studies on the cobalt(II) cyclidenes have involved alkyl groups at the R^2 position. Discovery that the R^3 methyl groups of those complexes having $R^2 = R^3 = CH_3$ are acidic (crystal structure on doubly deprotonated species[7]) led to the kinetic and mechanistic studies[6] that established the role of the deprotonated species. Replacement of the R^3 methyl group by phenyl results in a 20-fold retardation of the rate of autoxidation. However, the complexes do still undergo autoxidation, and the rates respond to base in a manner suggestive of the conjugate base mechanism.[6] The methyl groups at the R^4 positions are common to all structures and the most likely sites for deprotonation in those cases where NH and ionizable R^3 groups have been eliminated. We have therefore proposed that removal of this reactive site should retard the autoxidation of these important dioxygen carriers. The results are summarized here.

Experimental Section

Reagents and Starting Materials. The solvents and reagents used in these studies were reagent grade or better. Solvents were purified according to published methods. *N*-Methylimidazole (MeIm) was dried over barium oxide. Methanol, acetonitrile, and MeIm used in preparation of cobalt complexes were distilled under argon and degassed by successive freeze−pump−thaw cycles prior to use. 1,3-Diaminopropane was dried by repeated distillation over sodium metal. Triformylmethane was prepared according to the published procedure and was sublimed before use.[8] *N,N*′-Dimethyl-1, 8-diaminooctane was prepared according to ref 9, with the slight modification that the amount of sodium hydroxide added before extraction of the final product was 20 rather than 2 g (correcting a typographical error in the ref). Spectroscopic and electrochemical techniques, inert atmosphere manipulations, and the technique used for dioxygen affinity determinations have been described elsewhere.[9,10]

Kinetic measurements were performed at low temperatures (from −75 to −50 °C) using a Hi-Tech Scientific (England) CryoStopped-Flow instrument equipped with stainless steel plumbing and mixing cell, the latter having sapphire windows, connected to a PC computer with IS-2 Rapid Kinetic Software. The mixing cell was maintained to ±0.1 K, and mixing time is 2 ms. Kinetic measurements were performed on acetone solutions containing 0.5−1.5 M of 1-methylimidazole with various starting concentrations of the C6-bridged cobalt complex (7×10^{-6}−5×10^{-5} M) and dioxygen (7×10^{-6}−1×10^{-4} M) and a more limited concentration range for the C8 bridged complex. Dioxygen/nitrogen gas mixtures were generated using Tylan FC-260 mass flow controllers. The low concentrations of reagents necessary to slow down the reaction limited the available range of concentrations. Series of 8−12 shots run gave standard deviations within 10%, with overall reproducibility within 20%.

Autoxidation measurements were conducted in a pure dioxygen atmosphere in a sealed 1 cm quartz cell connected by graded seals to a Pyrex tube with a prefabricated neck. For autoxidation rate measurements, a temperature of 30 ± 0.3 °C was maintained for extended periods of time using an Abderhalden pistol with a 2-methylbutane/pentane mixture. Precautions were taken to prevent any possibility of acetonitrile/O_2 vapor explosions during sealing.

Syntheses. 2,2′-[Propylenebis(iminomethylidyne)]-1,3-propanedione (IIIa). Freshly sublimed triformylmethane[8] (30g, 0.3 mol) was dissolved in absolute ethanol (375 mL) with continuous stirring. The solution was placed in an ice bath, and anhydrous 1,3-diaminopropane (12.5 mL, 0.15 mol) was added dropwise with stirring at such a rate that the temperature did not exceed 30 °C. The solution became greenish-yellow and, after addition of approximately half of the 1,3-diaminopropane, a crystalline precipitate started to form. After addition was complete, the reaction mixture was refrigerated for several hours to crystallize the main portion of the product. The yellowish precipitate was removed by filtration, washed twice with absolute alcohol and once with ether, and dried *in vacuo* over P_4O_{10} for several hours. The mother liquor deposited additional product for 2 more days. Diethyl ether was then added to precipitate more product. The overall yield was 30.3 g (85%). The crude product is suitable for further reaction but can be purified by recrystallization from ethanol (*ca*. 50 mL/g). The melting point was 185−186 °C. Anal. Calcd for $C_{11}H_{14}N_2O_4$: C, 55.46; N, 11.76; H, 5.88. Found: C, 55.34; N, 11, 70; H, 6.10. FAB/TG-G 239 $[M + H]^+$. Spectral data are given in Table 1 and discussed later in this paper.

{2,2′-[Propylenebis(iminomethylidyne)]-1,3-propanedionato(2−)}nickel(II) Monohydrate (IVa). Ligand **IIIa** (21g, 88 mmol) and nickel(II) acetate 4-hydrate (21.8 g, 88 mmol) were stirred in 250 mL of ethanol for 16 h. A pale lavender precipitate was filtered, washed with ethanol, and dried *in vacuo* for several hours. Yield 24.0 g (87%). Calcd for $C_{11}H_{14}N_2O_5Ni$: C, 42.22; N, 8.95; H, 4.51. Found: C, 42.01; N, 8.70; H, 4.40. FAB/MB 295 $[M + H]^+$.

[7,15-Diformyl-1,5,9,13-tetraazacyclotetradeca-5,7,13,15-tetraenato-(2−)]nickel(II) (VIa). Complex **IVa** (24.0g, 77 mmol) was slurried in 120 mL of anhydrous 1,3-diaminopropane giving a color change from blue to violet. On heating the mixture at 160 °C for 0.5 h, the starting complex dissolved giving a brown solution. Approximately one-third of the 1,3-diaminopropane escaped by distillation during the heating. The resulting solution was poured into water (1200 mL), resulting in immediate formation of a green precipitate **V**. The mixture was then stirred for 24 h at room temperature, whereupon the precipitate gradually changed in color from green to red. The resulting precipitate

(6) Masarwa, M.; Warburton, P. R.; Evans, W. E.; Busch, D. H. *Inorg. Chem.* **1993**, *32*, 3826.

(7) Goldsby, K. A.; Jircitano, A. J.; Nosco, D. L.; Stevens, J. C.; Busch, D. H. *Inorg. Chem.* **1990**, *29*, 2523.

(8) Buděšinskỳ, M.; Fiedler, P.; Arnold, Z. *Synthesis* **1989**, 858.

(9) Thomas, R.; Fendrick, C. M.; Lin, W.-K.; Glogowski, M. W.; Chavan, M. Y.; Alcock, N. W.; Busch, D. H. *Inorg. Chem.* **1988**, *27*, 2534.

(10) Korybut-Daszkiewicz, B.; Kojima, M.; Cameron, J. H.; Herron, N.; Chavan, M. Y.; Jircitano, A. J.; Coltrain, B. K.; Neer, G. L.; Alcock, N. W.; Busch, D. H. *Inorg. Chem.* **1984**, *23*, 903.

Table 1. NMR and IR Spectral Parameters for the Synthetic Products

compd	solvent and ^{1}H NMR data (ppm)	solvent and ^{13}C NMR data (ppm)	selected infrared data (cm^{-1})
IIIa	$CDCl_3$: 1.89 (2H, m); 3.43 (4H, m); 7.85 (2H, br, as); 9.24 (2H, br); 9.53 (2H, br); 10.44 (2H, br)	$(CD_3)_2SO$: 30.6; 47.1; 111.3; 157.3 (br); 163.0 (br); 184.4 (br); 187.5; 190.5 (br)	3411; 3216 (s); 3178; 1640 (s); 1615 (s); 1428; 1309 (s); 1205 (s); 857
IVa	data not available due to paramagnetic properties	data not available due to paramagnetic properties	3408 (br); 3220; 1647; 1601 (s); 1542 (s); 1395; 1260; 1236
VIa	$CDCl_3$: 1.86 (4H, m); 3.26 (4H, m); 3.33 (4H, m); 6.92 (2H, s); 7.45 (2H, s); 9.08 (2H, s)	$CDCl_3$: r{27.1, 27.4, 27.6}; r{54.4, 54.6} 112.8; 156.6; 160.8; 186.8	3454 (br); 1646 (w); 1592 (vs); 1545; 1431; 1264; 1101
IXa	CD_3CN: 1.83 (4H, br); 2.97−3.16 (14H, m); 6.3 (br); 7.64 (2H, s); 7.70 (2H, s); 8.04 (2H, br s)	CD_3CN: 28.3; 35.9, 54.8; 61.8; 62.1; 107.8; 160.7; 161.5; 166.8	3384; 1658 (s); 1619 (vs); 1565; 1370; 1278; 838 (vs); 559
X[a]	CD_3CN: 1.38 (4H, br); 1.73 (4H, br); 2.00* (4H, br); 3.34 (6H, br); 3.58 (4H, t); 3.70 (8H, br); 7.47 (2H, s) 7.90 (2H, br d); 8.10 (2H, br d)	CD_3CN: 27.4; 29.2; 30.0; 42.0, 57.8; 58.7; 63.0; 107.4; 157.4; r{160.5;161.1}; r{163.1;163.8}	3425 (br); 2931; 1620 (vs); 1414; 839 (vs); 558
XI[a]	CD_3CN: 1.18−2.22* (16H, br m); 3.00−3.80 (18H, br m); 6.90−7.60 (6H, br m)	CD_3CN: 24.9; 25.1; 27.0; 29.9; r{38.0; 39.9; 42.3; 44.0}; r{52.0; 53.1; 42.3}; 56.5 (br); 61.5; 104.9; r{157.5; 158.5}; r{161.0; 162.2}; 163.4	3437 (br); 2937; 2860; 1619 (vs); 1563; 1452; 1115; 1373; 1273; 1137; 956; 838 (vs)
XII	CD_3CN: 1.23 (4H, br s); 1.60 (4H, br s); 2.05* (4H, br s); 3.20 (6H, s); 3.33 (4H, br s); 3.60 (8H, br t); 7.28 (2H, s); 7.70 (2H, br s); 8.25 (2H, br s); 11.5 (3H, br s)	CD_3CN: 27.1; 27.6; 28.7; 39.3; 53.1; 62.5; 162.9; 186.1	3430 (br); 2921; 1620 (vs); 1413; 1123; 839 (vs); 561
XIII	CD_3CN: 1.06−1.48 (12H, m); 1.92 (4H, m) 2.20−3.05 (18H, br m); 6.18 (2H, br s); 6.59 (2H, br s); 7.41 (2H, br s); 11.7 (3H, br s)	CD_3CN: 23.5; 27.1; 27.9; 28.3; 39.3; 53.1; 62.5; 162.1; 193.1	3436 (br); 2932; 2857; 1625 (vs); 1461; 1415; 1374; 1276; 1212; 1131; 842 (vs)
XIV	data not available due to paramagnetic properties	data not available due to paramagnetic properties	3443 (br); 1581 (vs); 1439; 1261; 1024; 848 (vs); 561
XV	data not available due to paramagnetic properties	data not available due to paramagnetic properties	3442 (br); 2932; 2859; 1618 (vs); 1571; 1438; 1416; 1373; 1273; 1200; 1136; 1077; 969; 844 (vs)
	*overlaps with residual acetonitrile signal; br, broad; s, singlet; d, doublet; t, triplet; m, multiplet	r, rotamer; br, broad	br, broad; w, weak; s, strong; vs, very strong

[a] NMR spectra will be discussed in a separate publication.

was isolated by filtration, washed with water, and dried in vacuo initially over $CaCl_2$ and later over P_4O_{10}. The crude product was dissolved in a minimum volume of chloroform and applied to a 5 × 25 neutral activated alumina column (Brockmann scale activity I). The mixture was eluted slowly with chloroform, discarding the first narrow green band. The second red-brown band was collected and evaporated on a rotary evaporator. The product was washed with ethanol and dried in vacuo. Yield 8.6 g (34%). Anal. Calcd for $C_{14}H_{18}N_4O_2Ni$: C, 50.49; N, 16.82; H, 5.45. Found: C, 50.40; N, 16.49; H, 5.80. FAB/MB 333 $[M]^+$ and 665 − cluster $[M_2 - H]^+$.

[3,11-Bis(methylaminomethylidene)-1,5,9,13-tetraazacyclohexadeca-1,4,9,12-tetraene-k^4*N*^{1,5,9,13}nickel(II)] Hexafluorophosphate (IXa). Complex **VIa** (1.0 g, 3 mmol) was suspended in 25 mL of dry methylene chloride, and methyl trifluoromethanesulfonate (1 mL, 8.8 mmol) was added (*caution, toxic reagent!*). The complex dissolved in a few minutes, giving a red-brown solution. The mixture was stirred for 16 h, after which 100 mL of 1.4 M methylamine in acetonitrile (140 mmol) was added. The mixture was stirred for 1 more h and then evaporated to approximately 1/5 of the initial volume. Ammonium hexafluorophosphate (2.5 g, 15 mmol) in methanol (20 mL) was added. The solution was evaporated to a small volume and refrigerated for several hours. The yellow crystalline product was filtered, washed with methanol, and dried in a vacuum oven for 2 h at 60 °C. Yield 1.1g (57%). Anal. Calcd for $C_{16}H_{26}N_6NiP_2F_{12}$: C, 29.52; N, 12.91; H, 4.03. Found: C, 29.16; N, 12.51; H, 4.35. FAB/NBA 505 $[M - PF_6]^+$ and 668 − $[M + H_2O]$.

(3,10-Dimethyl-3,10,14,18,21,25-hexaazabicyclo[10.7.7]hexacosa-1,11,13,18,20,25-hexaene-k^4*N*^{14,18,21,25})nickel(II) Hexafluorophosphate (X) and (3,12-Dimethyl-3,12,16,20,23,27-hexaazabicyclo[12.7.7]-hexacosa-1,13,15,20,22,27-hexaene-k^4*N*^{16,20,23,27})nickel(II) Hexafluorophosphate (XI). Complex **VIa** (2 g, 6 mmol) was suspended in 50 mL of dry methylene chloride, and methyl trifluoromethanesulfonate (2 mL, 18 mmol) was added (*caution, toxic reagent!*). The complex dissolved in a few minutes, giving a red-brown solution. The mixture was stirred for 16 h and the solvent was then removed on a rotary evaporator (with a KOH/MeOH trap to prevent methyl trifluoromethanesulfonate vapors from escaping). Copious foam formed at the final stages of evaporation, but periodical release of vacuum with dry air helped to prevent excessive foaming. The oily residue was then dried at 0.1 Torr, 50 °C for half an hour and then dissolved in 100 mL of dry acetonitrile. The corresponding aliphatic α,ω-diamine (6 mmol) was separately dissolved in 100 mL of dry acetonitrile. These two solutions were added at a rate of 10 mL h^{-1}, by means of a syringe pump to 1000 mL of stirred acetonitrile maintained under nitrogen at reflux temperature. After the addition was complete, the solvent was removed by rotary evaporation to give a viscous dark red-brown residue. Ammonium hexafluorophosphate (2.0 g, 12 mmol) in methanol (17 mL) was added, and the resulting solution was applied to a 2 × 25 cm silica (70−230 mesh, 60 Å) column. The first orange bands (*ca*. 75 mL for **X** and *ca*. 250 mL for **XI**) were separated from the next brown bands. The fractions were evaporated to small volumes, and several milliliters of methanol were added. Solvent evaporation-methanol addition cycles were repeated 2−3 times until crystallization occurred. The products were filtered, washed twice with methanol, and dried in vacuo for several hours. Yields: 0.67 g (15%) for **X** and 1.24 g (27%) for **XI**. Anal. Calcd for $C_{22}H_{36}N_6NiP_2F_{12}$: C, 36.06; N, 11.46; H, 4.95. Found: C, 35.68; N, 11.41; H, 4.99. FAB/NBA: 443 $[M - 2PF_6]$ and 587 − $[M - PF_6]$. Anal. Calcd for $C_{24}H_{40}N_6NiP_2F_{12}$: C, 37.87; N, 11.04; H, 5.30. Found: C, 37.64; N, 11.02; H, 5.45. FAB/NBA: 470 $[M - 2PF_6]$ and 615 − $[M - PF_6]$.

(3,10-Dimethyl-3,10,14,18,21,25-hexaazabicyclo[10.7.7]hexacosa-1,11,13,18,20,25-hexaene) Hexafluorophosphate (XII) and (3,12-Dimethyl-3,12,16,20,23,27-hexaazabicyclo[12.7.7]hexacosa-1,13,15,20,22,27-hexaene) Bis(hexafluorophosphate) Chloride (XIII). Anhydrous hydrogen chloride was bubbled through 5 × 10^{-2} M solutions of **X** or **XI** in acetonitrile. Higher concentrations are not recommended since the tar-like consistency of the precipitates described below prevents complete Ni^{2+} removal. After several seconds of bubbling, the solutions have changed in color from yellow-orange to turquoise blue. In a few more seconds a turquoise precipitate forms and almost immediately redissolves. At this stage, bubbling of

hydrogen chloride was stopped. The solvent was removed by rotary evaporation at room temperature. The resulting gummy residues were carefully washed several times with water to obtain a negative test for nickel(II) with dimethylglyoxime. The off-white precipitates were dried over $CaCl_2$ *in vacuo*. Yields: 68% for **XII** and 56% for **XIII**. Anal. Calcd for $C_{22}H_{39}N_6P_3F_{18}$: C, 32.13; N, 10.22; H, 4.78. Found: C, 32.66; N, 10.18; H, 5.01. FA B/NBA: 385 [M − $3PF_6$]; 531 [M − $2PF_6$] and 675 − [M − PF_6]. Anal. Calcd for $C_{24}H_{43}N_6P_2F_{12}Cl$: C, 38.90; N, 11.34; H, 5.85. Found: C, 39.78; N, 11.63; H, 5.90. FAB/NBA: 413 [M − $2PF_6$ − Cl] and 559 − [M − PF_6 − Cl].

(3,10-Dimethyl-3,10,14,18,21,25-hexaazabicyclo[10.7.7]hexacosa-1,11,13,18,20,25-hexaene-k^4*N*^{14,18,21,25})(methanol)cobalt(II) Hexafluorophosphate (XIV) and (3,12-Dimethyl-3,12,16,20, 23,27-hexaazabicyclo[12.7.7]hexacosa-1,13,15,20,22,27-hexaene-k^4*N*^{16,20,23,27})-(methanol)cobalt(II) Hexafluorophosphate (XV). These preparations were carried out in an inert atmosphere glovebox using degassed dry methanol. The ligand salt **XII** or **XIII** (1 mmol) was slurried in methanol (20 mL), and the mixture was heated to boiling. A solution containing cobalt(II) acetate 4-hydrate (0.249 g, 1 mmol) and sodium acetate 3-hydrate (0.136 g, 1 mmol) in 10 mL of hot methanol was added to the suspension. After several minutes the ligand salt dissolved, and the color changed to a deep orange. The volume of the solution was reduced to approximately one-half, and the reaction mixture was left to crystallize. Crystallization was complete in about 30 min for **XIV** and in several hours for **XV**. The products were washed with methanol and dried in the glovebox. Crystals of **XV** gradually turn opaque upon removal from the mother liquor due to loss of methanol. Yields: 0.46 g (63%) for **XIV** and 0.47 g (62%) for **XV**. Anal. Calcd for $C_{23}H_{40}N_6OCoP_2F_{12}$: C, 36.09; N, 10.98; H, 5.27. Found: C, 36.38; N, 11.68; H, 5.20. FAB/NBA: 443 [M − $2PF_6$] and 588 − [M − PF_6]. Anal. Calcd for $C_{25}H_{44}N_6OCoP_2F_{12}$: C, 37.84; N, 10.59; H, 5.59. Found: C, 37.57; N, 10.64; H, 5.60. FAB/NBA: 471 [M − $2HPF_6$] and 616 − [M − PF_6].

X-ray Structural Analysis. Crystal Data: $C_{23}H_{40}N_6OCoP_2F_{12}$, M = 765.5, monoclinic, $P2_1/c$, a = 19.053(13), b = 12.419(7), c = 14.635(7) Å, β = 109.95(5)°, U = 3255 Å^3, Z = 4, D_c = 1.56 g cm^{-3}, Mo Kα radiation, λ = 0.71069 Å, μ (Mo Kα radiation) = 0.72 mm^{-1}, T = 200 K.

Data were collected with a Siemens R3m four circle diffractometer in ω-2θ mode. The crystal was held at 200 K with an Oxford Cryosystems Cryostream Cooler.[11] Maximum 2θ was 45° with scan range ±0.7°(ω) around the K_{a1}-K_{a2} angles, scan speed 3−15°(ω) min^{-1}, depending on the intensity of a 2 s prescan; backgrounds were measured at each of the scans for 0.25 of the scan time. *hkl* ranges were −1/15; −1/13; and −19/19. Three standard reflections were monitored every 200 reflections and showed a slight decrease (2%) during data collection. The data were rescaled to correct for this. Unit cell dimensions and standard deviations were obtained by least-squares fit to 15 reflections (7° < 2θ < 16°). Reflections were processed using profile analysis to give 4264 unique reflections (R_{int} = 0.046), of which 1496 were considered observed ($I/\sigma(I)$ > 2.0). These were corrected for Lorentz, polarization, and absorption effects (by the analytical method using ABSPSI[12]); minimum and maximum transmission factors were 0.88 and 0.91. Crystal dimensions were 0.23 × 0.31 × 0.17 mm.

Systematic reflection conditions: *h*0*l*, *l* = 2*n*; 0*k*0, *k* = 2*n* indicate space group $P2_1/c$. The structure was solved (with difficulty on account of the weak data) by direct methods using SHELXTL (TREF). Further light atoms were then found by E-map expansion and successive Fourier syntheses. One PF_6 group was extensively disordered and was approximately modeled by two sets of fluorine atoms with occupancies 0.7 and 0.3. It was necessary to constrain the C−C distances along the polymethylene chain, to keep the refinement and anisotropic displacement parameters stable (refining the 1−2 and 1−3 C−C distances). Anisotropic displacement parameters were used for all non-H atoms (apart from the minor fluorine atoms and one carbon atom which proved unstable on refinement and was held isotropic). Hydrogen atoms were given fixed isotropic displacement parameters, U = 0.08 Å^2. Those defined by the molecular geometry were inserted at calculated positions and not refined; methyl groups were treated as rigid CH_3 units, with their initial orientation based on a staggered configuration. Final refinement was on F by least squares methods refining 426 parameters. Largest positive and negative peaks on a final difference Fourier synthesis were of height 0.7 and −0.5 el. Å^{-3}.

A weighting scheme of the form $W = 1/(\sigma^2(F) + gF^2)$ with g = 0.000 24 was used and shown to be satisfactory by a weight analysis. Final R = 0.085, R_w = 0.076, S = 2.11; R for all reflections = 0.257. Maximum shift/error in final cycle was 0.05. The relatively high R-value is readily understandable in the light of the weak scattering and the severe disorder of the anions.

Computing was with SHELXTL PLUS[13] on a DEC Microvax-II. Unusually, refinement on all reflections with SHELXL proved unstable, apparently because of anomalously strong weak reflections; this is attributed to scattering from minor twin components of the crystal selected. Scattering factors in the analytical form and anomalous dispersion factors were taken from ref 14 (stored in the program). Final atomic coordinates are given in supporting information and selected bond lengths and angles in Table 2.

Table 2. Selected Bond Lengths (Å) and Angles (deg) for [Co(C6MeHH[16]cyclidene)·CH_3OH]$(PF_6)_2$ (**XIV**)

Co(1)−N(1)	1.951(14)	Co(1)−N(5)	1.958(15)
Co(1)−N(9)	1.916(14)	Co(1)−N(13)	1.921(14)
Co(1)−O(30)	2.209(12)	N(1)−C(2)	1.490(20)
N(1)−C(16)	1.321(21)	N(5)−C(4)	1.493(22)
N(5)−C(6)	1.279(29)	N(9)−C(8)	1.284(28)
N(9)−C(10)	1.475(26)	N(13)−C(12)	1.516(29)
N(13)−C(14)	1.308(22)	N(18)−C(17)	1.280(25)
N(18)−C(19)	1.502(29)	N(18)−C(20)	1.511(35)
N(26)−C(25)	1.484(23)	N(26)−C(27)	1.290(21)
N(26)−C(28)	1.496(27)	C(2)−C(3)	1.509(29)
C(3)−C(4)	1.508(27)	C(6)−C(7)	1.394(25)
C(7)−C(8)	1.498(31)	C(7)−C(27)	1.367(29)
C(10)−C(11)	1.501(23)	C(11)−C(12)	1.529(27)
C(14)−C(15)	1.428(29)	C(15)−C(16)	1.405(24)
C(15)−C(17)	1.399(26)	C(20)−C(21)	1.460(49)
C(21)−C(22)	1.455(32)	C(22)−C(23)	1.469(38)
C(23)−C(24)	1.464(26)	C(24)−C(25)	1.456(23)
O(30)−C(31)	1.391(26)		
N(1)−Co(1)−N(5)	89.5(7)	N(1)−Co(1)−N(9)	165.1(7)
N(5)−Co(1)−N(9)	88.9(7)	N(1)−Co(1)−N(13)	91.4(7)
N(5)−Co(1)−N(13)	166.8(7)	N(9)−Co(1)−N(13)	86.9(7)
N(1)−Co(1)−O(30)	94.6(6)	N(5)−Co(1)−O(30)	97.4(5)
N(9)−Co(1)−O(30)	100.4(6)	N(13)−Co(1)−O(30)	95.6(6)
Co(1)−N(1)−C(2)	121.4(10)	Co(1)−N(1)−C(16)	120.2(12)
C(2)−N(1)−C(16)	118.2(14)	Co(1)−N(5)−C(4)	118.2(13)
Co(1)−N(5)−C(6)	120.7(12)	C(4)−N(5)−C(6)	120.9(16)
Co(1)−N(9)−C(8)	121.1(14)	Co(1)−N(9)−C(10)	122.1(13)
C(8)−N(9)−C(10)	116.4(15)	Co(1)−N(13)−C(12)	122.2(11)
Co(1)−N(13)−C(14)	119.6(14)	C(12)−N(13)−C(14)	118.2(15)
C(17)−N(18)−C(19)	122.1(21)	C(17)−N(18)−C(20)	124.4(19)
C(19)−N(18)−C(20)	112.6(17)	C(25)−N(26)−C(27)	130.1(19)
C(25)−N(26)−C(28)	111.9(14)	C(27)−N(26)−C(28)	117.8(15)
N(1)−C(2)−C(3)	111.9(15)	C(2)−C(3)−C(4)	114.5(17)
N(5)−C(4)−C(3)	109.8(13)	N(5)−C(6)−C(7)	125.1(20)
C(6)−C(7)−C(8)	115.2(20)	C(6)−C(7)−C(27)	114.0(19)
C(8)−C(7)−C(27)	128.5(16)	N(9)−C(8)−C(7)	122.9(17)
N(9)−C(10)−C(11)	112.1(14)	C(10)−C(11)−C(12)	114.3(14)
N(13)−C(12)−C(11)	105.2(18)	N(13)−C(14)−C(15)	124.6(16)
C(14)−C(15)−C(16)	120.7(16)	C(14)−C(15)−C(17)	123.0(16)
C(16)−C(15)−C(17)	115.6(18)	N(1)−C(16)−C(15)	123.5(18)
N(18)−C(17)−C(15)	128.3(22)	N(18)−C(20)−C(21)	100.3(20)
C(20)−C(21)−C(22)	114.7(27)	C(21)−C(22)−C(23)	113.7(22)
C(22)−C(23)−C(24)	113.1(19)	C(23)−C(24)−C(25)	114.2(17)
N(26)−C(25)−C(24)	113.9(17)	N(26)−C(27)−C(7)	126.6(16)
Co(1)−O(30)−C(31)	126.0(10)		

(11) Cosier, J.; Glaser, A. M. *J. Appl. Cryst.* **1986**, *19*, 105.
(12) Alcock, N. W.; Marks, P. J. *J. Appl. Cryst.* **1994**, *27*, 200.
(13) Sheldrick, G. M. SHELXTL PLUS User's Manual; Nicolet Instr. Co.: Madison, WI, 1986.
(14) International Tables for X-ray Crystallography; Kynoch Press: Birmingham, 1974; Vol. IV (Present distributor Kluwer Academic Publishers, Dordrecht).

Scheme 1. Selected Synthetic Transformations in Cyclidene Chemistry

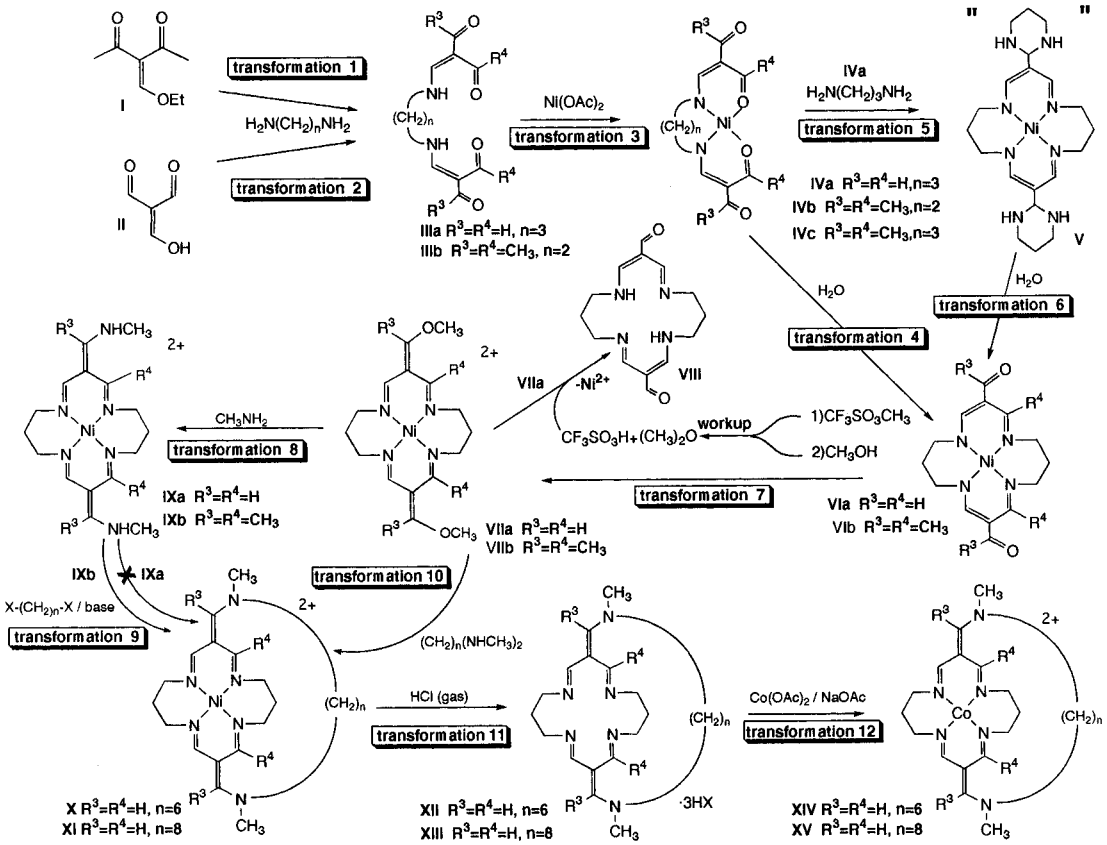

Results and Discussion

Synthesis and Characterization. A general synthetic scheme showing the numbering of the materials and the sequential steps is given in Scheme 1. Newly prepared materials were routinely characterized and identified by analysis, ^{13}C and ^{1}H NMR, FAB MS, and IR (Table 1 and procedures). In general, the synthetic route to unsubstituted cyclidenes was patterned after that for the substituted analogs,[9,10,15] (Scheme 1), but differences abound, and they start with a change in the initial starting material. 3-(Ethoxymethylene)-2, 4-pentanedione (**I**) (Scheme 1) used for all previous cyclidene syntheses necessarily gives products with $R^3 = R^4 = CH_3$. Triformylmethane, which is the essential reagent, has recently been prepared and characterized (sublimed white solid, mp = 104−106 °C).[8] Triformylmethane mainly exists in solution in the enol form (**II**) with a structure similar to that of 3-(ethoxymethylene)-2,4-pentanedione (**I**).

The first ligand produced by condensation, 2,2′-[propylenebis-(iminomethylidyne)]-1,3-propanedione (**IIIa**), prepared in analogy to its well-known counterpart, 3,3′-[ethylenebis(iminomethylidene)]di-2,4-pentanedione (**IIIc**),[15a] was found by FAB/TG-G mass-spectra ([M + H] peak $m/z = 239$) to contain the macrocyclic byproduct **VIII** ($m/z = 279$). Conveniently, both **IIIa** and its impurity **VIII** give the desired macrocyclic complex **VIa** via transformations 3, 5, and 6 (Scheme 1). ^{13}C and ^{1}H NMR spectra suggest that solutions of **IIIa** are mixtures of at least two different tautomers containing either aldehyde or enol forms of the molecule. Interconversion of these forms causes substantial broadening of the NMR peaks.

The physical properties of the open-chain unsubstituted nickel(II) complex (**IVa**), prepared by reaction of ligand **IIIa** with nickel(II) acetate 4-hydrate, differ substantially from those of its methyl substituted analogs **IVb** and **IVc**.[15a,16] The latter are typical diamagnetic orange or brown, pseudosquare planar nickel(II) complexes. **IVa** has a rather pale lavender color and a magnetic moment of 3.17 μ_B which are well-known characteristics of octahedral nickel(II). These properties, its low solubility, and a composition that does not allow other ligands all point to an oligomeric structure involving bridging by the exocyclic aldehyde groups, in analogy to the previously described polymeric benzoyl substituted copper complexes.[17]

Another significant difference between the preparation of the macrocyclic nickel(II) complex **VIa** and those of its substituted analogs (**VIb**, for example) is the formation of the intense green side-product/intermediate **V** (transformation 5). This material precipitates on addition of water to the 1,3-diaminopropane solution and undergoes slow hydrolysis to **VIa** (transformation 6). Continuing the uniqueness of the *unsubstituted* systems, the macrocyclic Jäger-type complex (**VIa**) was obtained, after lengthy workup, as a bright-red microcrystalline solid in contrast with its yellow orange congenors.

Methylation of the carbonyl group of the Jäger complex **VIb** (transformation 7) is a critical step that facilitates the synthesis of the macrobicyclic lacunar ligands. The reaction commonly makes use of an excess of a powerful methylating agent (methyl trifluoromethanesulfonate, methyl fluorosulfate, or trimethyloxonium tetrafluoroborate), followed by subsequent decomposition of the excess methylating agent with methanol.[15b,c] The

(15) (a) Riley, P. R.; Busch, D. H. *Inorg. Synth.* **1978**, *18*, 36. (b) Cairns, C. J.; Busch D. H. *Inorg. Synth.* **1990**, 27, 261. (c) Busch, D. H.; Olszanski, D. J.; Stevens, J. C.; Schammel, W. P.; Kojima, M.; Herron, N.; Zimmer, L. L.; Holter, K. A.; Mocak, J. *J. Am. Chem. Soc.* **1981**, *103*, 1472. (d) Busch, D. H.; Christoph, G. G.; Zimmer, L. L.; Jackels, S. C.; Grzybowski, J. J.; Callahan, R. C.; Kojima, M.; Holter, K. A.; Mocak, J.; Herron, N.; Chavan, M.; Schammel, W. P. *J. Am. Chem. Soc.* **1981**, *103*, 5107. (e) Busch, D. H.; Jackels, S. C.; Callahan, R. C.; Grzybowski, J. J.; Zimmer, L. L.; Kojima, M.; Olszanski, D. J.; Schammel, W. P.; Stevens, J. C.; Holter, K. A.; Mocak, J. *Inorg. Chem.* **1981**, *20*, 2834.

(16) Jäger, E. *Z. Chem.* **1968**, *8*, 392.

(17) Jäger, E. *Z. Anorg. Allg. Chem.* **1966**, *346*, 76.

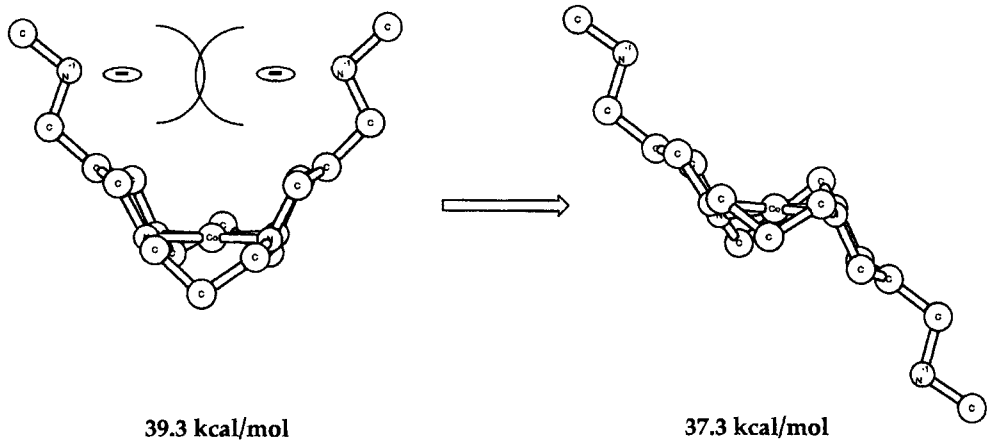

Figure 2. Hypothetical U-Z isomerization (Lin, W.-K.; Alcock, N. W.; Busch, D. H. *J. Am. Chem. Soc.* **1991**, *113*, 7603) of the dianion IXa.

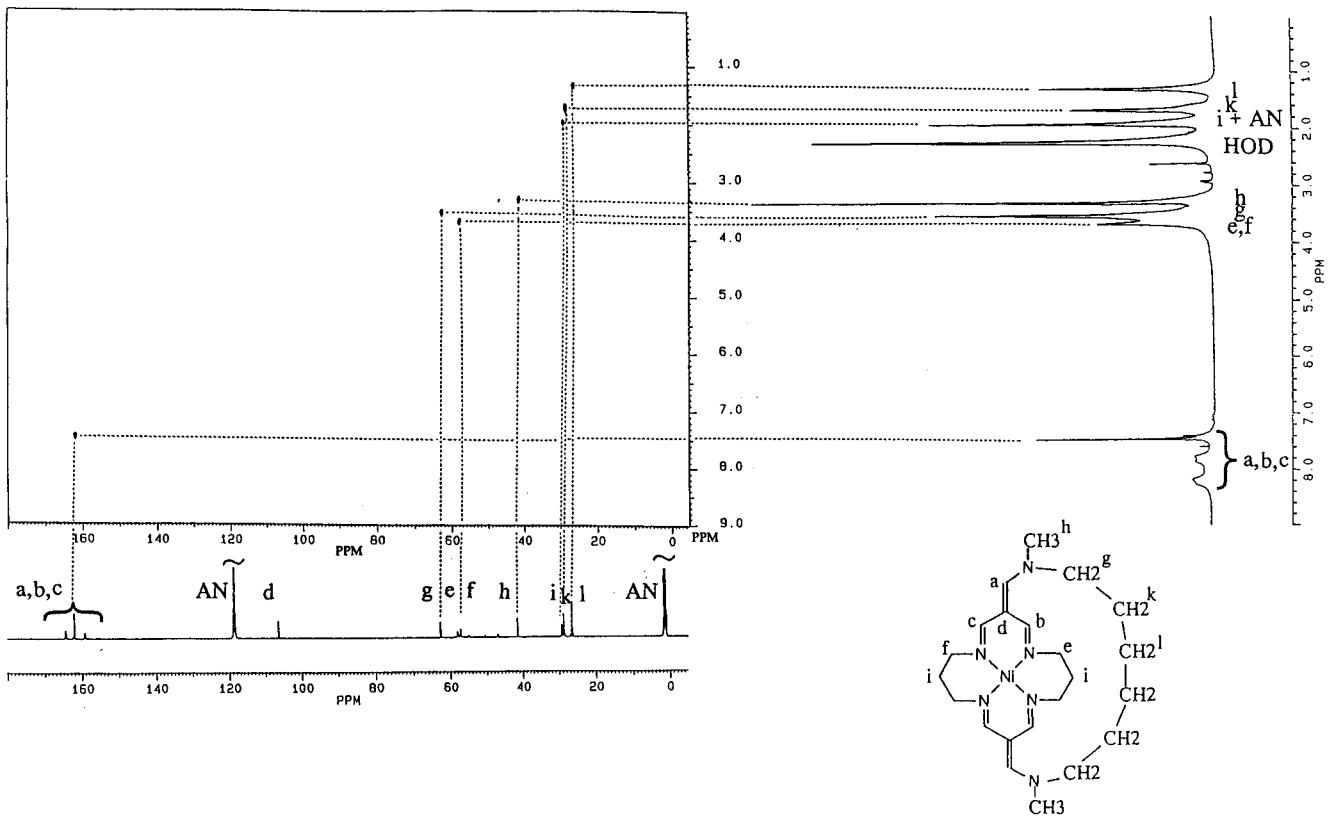

Figure 3. The HETCOR spectrum of [Ni(C6MeHH[16]cyclidene)]$(PF_6)_2$ (**X**) in CD_3CN. Dots that appear in front of the strong acetonitrile signal at about 120 ppm and are not connected by dotted lines appeared due to the leakage of radio frequency.

previously known methoxyethylidene substituted macrocyclic complexes (e.g., **VIIb**) are crystalline, reasonably stable materials. In contrast, for the unsubstituted complex **VIIa**, the addition of methanol leads to decomposition, even though the presence of the bis-methylated complex **VIIa** was confirmed by FAB/NBA. An unseparated mixture of the methylated products was therefore used in the next stage, after distilling off the excess of methyl trifluoromethylsulfonate (transformation 10).

Final ring closure also provided its challenges. For substituted cyclidenes the second ring closure could be performed either by reaction of the bismethylamino-derivative **IXb** with α,ω-ditosylalkanes (transformation 9) or by the direct reaction of bis(methoxyethylidene) macrocycle **VIIb** with diamines (transformation 10).[15b,c] For the unsubstituted complexes, the first approach was initially investigated, since complex **IXa** was available, but extensive studies gave exclusively unbridged products with hexamethylene or decamethylene chains attached on only one side. A rationale for this difference in behavior is visualized in Figure 2. Earlier X-ray structural and molecular mechanics studies have shown that the saddle or U-shaped conformation is generally preferred for neutral substituted [16]-cyclidene complexes. However, deprotonation of the two methylamine moieties produces a dianionic ligand, and the Z-conformation may be more stable than the U-conformation. Obviously the Z-isomer cannot undergo a bridging reaction with an α,ω-ditosylalkane.

Nickel cyclidenes **X** and **XI**, containing the final desired ligand, were prepared in 15 and 27% yields, respectively, using an alternative cyclization route based on the reaction of aliphatic hexamethylenediamine or octamethylenediamine with crude **VIIa** (transformation 10). The monomeric bicyclic structures of the products were confirmed by mass spectrometry and NMR results (e.g., Figure 3).

Demetalation approximated the known procedure (transformation 11),[15b] giving **XII** as an off-white solid tris(hexafluorophosphate) salt and **XIII** as a mixed chloride-hexafluoro-

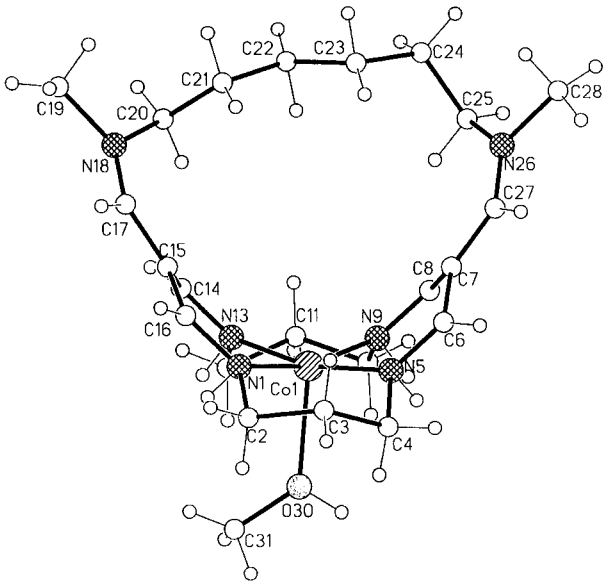

Figure 4. X-ray structure and atom numbering for [Co(C6MeHH[16]-cyclidene)(CH_3OH)] cation (**XIV**).

phosphate, compositions consistent with earlier work.[15b] The ultimate products, the unsubstituted cobalt(II) complexes **XIV** and **XV**, were prepared by the procedure for the corresponding methyl substituted cobalt(II) cyclidenes and differed only in that the crystals contained one or three molecules of coordinated methanol.

Structure of Complex [Co(C6MeHH[16]cyclidene)(CH_3OH)](PF_6)$_2$ (XIV). The complex exhibits (Figure 4) the typical saddle shaped lacunar structure that has been well documented for the 16-membered cyclidenes.[1b,18] Comparison with the structures of [Co(C6MeMeMe[16]cyclidene)]$^{2+}$ and related compounds reveals a profound example of structural changes caused by vicinal repulsion (Figure 5a). In the structure of [Co(C6MeHH[16]cyclidene)]$^{2+}$ coordinated methanol leads to the displacement of the cobalt atom from the plane of the four nitrogens by 0.23 Å (compared to 0.06 Å in the substituted species). Also, methanol coordination causes both saturated chelate rings to assume the chair conformation, a behavior typical of cyclidenes with axial ligands.[1b] The macrocyclic backbones of [Co(C6MeHH[16]cyclidene)]$^{2+}$ and [Co(C6MeMeMe[16]-cyclidene)]$^{2+}$ have approximately the same dimensions.[18b] Substantially different widths occur between exocyclic nitrogens and an even greater variation in the distances between bridge terminal carbons (T) (Table 3). Data for the dioxygen adduct of [Co(C6MeMeMe[16]cyclidene)]$^{2+}$ are included to emphasize the fact that two bridge conformations exist for the subsituted (R^4 = methyl) complex, depending on whether the cavity is filled or vacant.

The conformations of the polymethylene bridges (drawn in Figure 5b−d) constitute the greatest and most important differences between [Co(C6MeHH[16]cyclidene)]$^{2+}$, [Co(C6MeMeMe[16]cyclidene)]$^{2+}$. Both conformations are unsymmetrical; a symmetrical conformation for polymethylene bridges with an even number of links (n) is possible only if the central carbon−carbon bond has a high energy, completely eclipsed conformation.[18b] In contrast to the folding of the bridge into its own cavity for [Co(C6MeMeMe[16]cyclidene)]$^{2+}$ (Figure 5c), a conformation featuring mostly *gauche* torsional angles, the conformation found for the unsubstituted complex contains a majority of low energy *anti* torsional angles (Figure 5b).

Differences in the twist of the $CH_3N(CH_2-)$ fragment around the nitrogen-vinyl carbon bond (ϵ, Table 3), seem to be the source of the conformational differences between the bridges for these two complexes, with values of 0° and 22° for [Co(C6MeHH[16]cyclidene)]$^{2+}$ and [Co(C6MeMeMe[16]cyclidene)]$^{2+}$, respectively (Table 3). This difference can be attributed to the absence or presence of steric repulsion between the R^2 and R^3 methyl groups. This repulsion forces the $CH_3N(CH_2-)$ units to rotate inwards, toward the cavity, reducing the overall bridge length. The absence of this repulsion favors a straighter bridge featuring low energy anti torsion angles. Therefore, it may be anticipated that elimination of the R^2/R^3 steric repulsion in [Co(C6MeHH[16]cyclidene)]$^{2+}$ makes bridge folding more difficult and generates more strain in the oxygenated complex.

Electrochemistry. Comparison of electrochemical data for nickel and cobalt cyclidenes (Table 4) provides a useful distinction between electronic and steric effects arising from ligand modifications. Earlier work[19] has shown that the redox potentials (M(III)/M(II)) of the nickel cyclidene complexes are insensitive to bridge length and only dependent on electronic factors, while the redox potentials of the cobalt complexes respond to both. This difference arises because of the tendency of cobalt to bind solvent molecules, especially in the trivalent state where 6-coordination is dominant. Since the ligand providing the sixth donor atom must go into the cavity, formation of the six-coordinate cobalt(II) complex depends on bridge length and cavity size. For cobalt complexes with identical sets of substituents R^2-R^4 but different bridge lengths (Table 4, entries 1, 5, 9, 14, 18 or 4, 8, 12, 17) redox potential gradually decreases as bridge length increases. For nickel, replacement of an electron donating methyl groups at R^2 and/or R^3 by hydrogen or phenyl causes an increase in redox potential. The unsubstituted cobalt cyclidenes, [Co(C6MeHH[16]cyclidene)]$^{2+}$ and [Co(C8MeHH[16]cyclidene)]$^{2+}$, display irreversible voltammograms with poorly defined reductive processes, and redox potentials of $\sim$0.53 and $>$0.41, respectively, indicating weak sixth ligand binding.[19] The high redox potentials are clearly associated with the replacement of the electron donating methyl group by hydrogen, but they almost certainly also reflect a decreased ability to bind the sixth axial ligand because of the distinctive bridge conformation.

ESR Spectra. The unoxygenated, unsubstituted cobalt(II) cyclidenes in acetonitrile/MeIm solution display an axial ESR pattern typical of many cobalt(II) cyclidenes (Figure 6).[20−22] Comparison of ESR spectral parameters for oxygenated unsubstituted cobalt(II) cyclidenes with previously published data supports the generalization that values for $g_\perp$ are extremely similar for dioxygen adducts of all cobalt cyclidenes (Table 5). Values for $g_\parallel$, $A_\perp$, and $A_\parallel$ are somewhat smaller than those for cyclidenes alkyl substituted at R^2 and/or R^3 and correspond to the spectral parameters of cyclidenes which lack electron donating substituents at these positions.[22] Thus, the electrochemical and ESR data both indicate a decrease in electron

(18) (a) Alcock, N. W.; Lin, W.-K.; Jircitano, A.; Mokren, J. D.; Corfield, P. W. R.; Johnson. G.; Novotnak, G.; Cairns, C.; Busch, D. H. *Inorg. Chem.* **1987**, *26*, 440. (b) Alcock, N. W.; Lin, W.-K.; Cairns, C.; Pike, G. A.; Busch, D. H. *J. Am. Chem. Soc.* **1989**, *111*, 6630.

(19) Chavan, M. Y.; Meade, T. J.; Busch, D. H.; Kuwana, T. *Inorg. Chem.* **1986**, *25*, 314.

(20) Busch, D. H.; Stephenson, N. A. Inclusion Compounds Volume 5: Inorganic and Physical Aspects of Inclusion; Atwood, J., Davies, E., MacNicol, D., Eds.; Oxford University Press: Oxford, 1991; pp 276−310.

(21) Drago, R. S.; Corden, B. B. *Acc. Chem. Res.* **1980**, *13*, 353.

(22) Busch, D. H. In *Oxygen Complexes and Oxygen Activation by Transition Metals*; Martell, A. E., Sawyer, D. T., Eds.; Plenum Publishing Corporation: 1988.

Table 3. Structural Parameters for Co(C6MeMeMe[16]cyclidene)$^{2+}$, Its MeIm/O_2 Adduct, and Co(C6MeHH[16]cyclidene)$^{2+}$

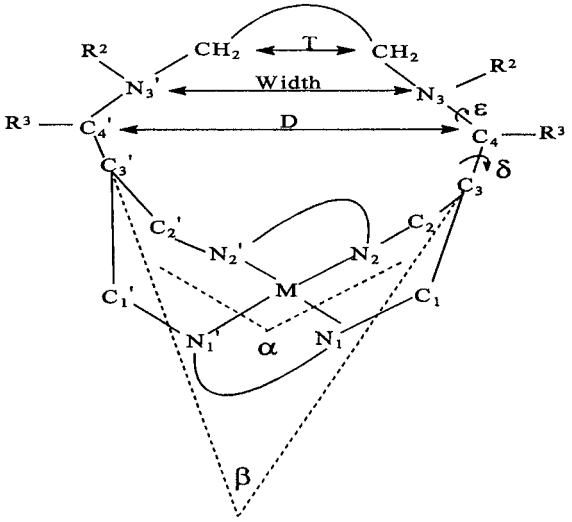

	α^0	β^0	δ^0	ϵ^0	D, Å	T, Å	width, Å	height, Å	chain conformations $C_1-C_2-C_3-C_4-C_5-C_6$[b]
CoC6MeMeMe[16]cyclidene^{2+} [a]	98.8	44.5	−23.43 27.80	−22.32 13.23	6.63	4.92	6.74	5.13	g_1-a-g_2-g_2-g_2
CoC6MeMeMe[16]cyclidene (MeIm)$(O_2)^{2+}$ [a]	110.6	55.8	−6.68 75.90	−114.2 −23.18	6.97	4.76	6.76	5.91	(g_2)-e_2-e_1-g_1-a
CoC6MeHH[16]cyclidene^{2+}	93.3	44.4	−29.43 25.33	−0.4 20.8	6.65	5.49	6.99	5.48	a-(a)-a-(e_2)-g_2

[a] Reference 18b. [b] The idealized labeling system is defined as follows, in the order torsional angle, label, type: 60, g_1, gauche; 120, e_1, eclipsed; 180, a, anti; −120, e_2, eclipsed; −60, g_2, gauche. Parentheses indicate substantial deviation from ideal angle. Structural parameters defining the cyclidene unit: α, angle between opposite [$N_1N_2C_1C_2$] planes; β, angle between opposite [$C_1C_2C_3$] planes; δ, torsion angle $C_2C_3C_4N_3$; ϵ, torsional angle $C_3C_4N_3CH_2$; D, distance C_3-C_3'; width, N_3-N_3' distance; T, distance between bridge terminal CH_2 groups.

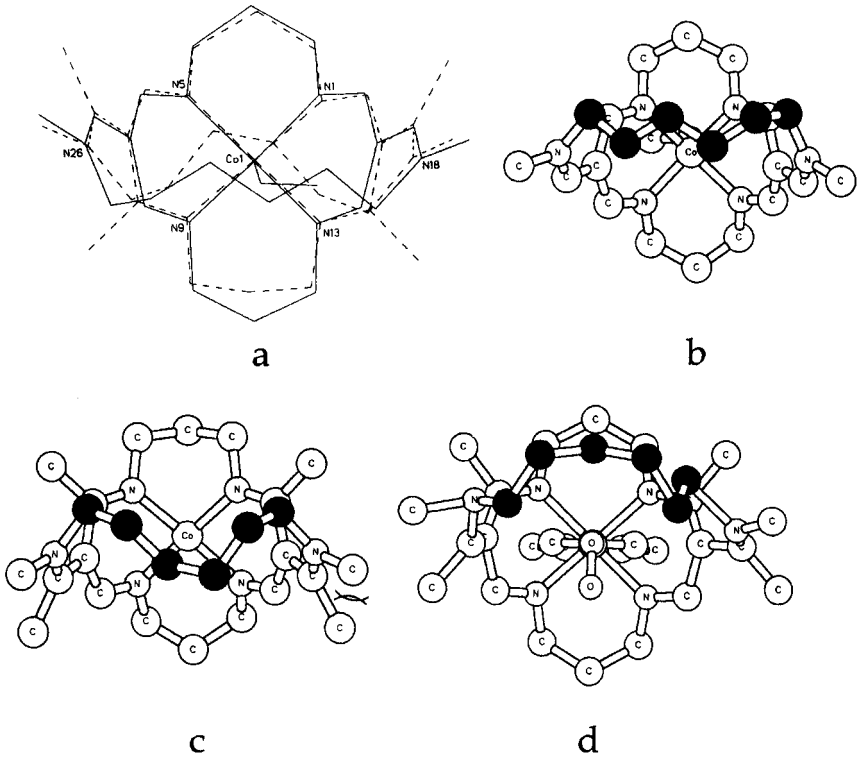

Figure 5. Bridge conformations from the X-ray structures: (a) Comparison of CoC6MeHH (**XIV**) (solid line) and the corresponding substituted species CoC6MeMeMe (dashed line) view from below; (b) [Co(C6MeHH[16]cyclidene)(CH_3OH)] cation; (c) [Co(C6MeMeMe[16]cyclidene)] cation; and (d) [Co(C6MeMeMe[16]cyclidene)MeIm(O_2)] cation.

density at the cobalt atom due to the absence of electron donating R^3 and/or R^4 substituents.

Dioxygen Affinities. The spectral changes used in the determination of dioxygen affinities (Figure 7) are completely reversible, and they show two isosbestic points, at 385 and 490 nm, suggesting a simple equilibrium involving only two absorbing species. Both of the unsubstituted cobalt(II) cyclidenes reported here have unusually low dioxygen affinities in

Table 4. Selected Redox Potentials for Nickel and Cobalt Cyclidenes[a]

	$R^1R^2R^3R^4$	$E_{1/2}$ (M = Ni)[b]	$E_{1/2}$ (M = Co)[b]	refs
1	C4MeMeMe	0.77	0.34	19, 15e
2	C4HMeMe	0.84		15e
3	C4HPhMe	0.90		10
4	C4MePhMe	0.91	0.50	10, 20
5	C5MeMeMe	0.76	0.28	15e, 19
6	C5HMeMe	0.85		15e
7	C5HPhMe	0.92		10
8	C5MePhMe	0.91	0.44	10, 20
9	C6MeMeMe	0.775	0.20	15e, 19
10	C6HMeMe	0.895		15e
11	C6MeHMe	0.97		10
12	C6MePhMe	0.92	0.34	10, 20
13	C6MeHH	0.87	0.53	this paper
14	C7MeMeMe	0.74	0.08	15e, 19
15	C7HMeMe	0.82		15e
16	C7HPhMe	0.92		10
17	C7MePhMe	0.90	0.24	10, 20
18	C8MeMeMe	0.78	0.05	15e, 19
19	C8HMeMe	0.84		15e
20	C8HPhMe	0.95		10
21	C8MeHH	0.87	>0.41	this paper

[a] In acetonitrile solution containing 0.1 M Nbu_4BF_4. [b] For the M(III)/M(II) redox couple.

Table 5. ESR Parameters[a] for Square Pyramidal, Low-Spin Cobalt(II) Complexes of Unsubstituted Cyclidenes and Their Dioxygen Adducts

$R^1R^2R^3R^4$	$g_{\|\|}$	$g_\perp$	$A_{\|\|}$ (G)	$A_\perp$ (G)	a_N
Square Pyramidal Complexes					
C6MeHH	2.009	2.312	91.0		14
C8MeHH	2.012	2.319	96.0		14
Dioxygen Adducts					
C6MeHH	2.084	2.001	16.8	8.6	
C8MeHH	2.083	2.001	16.1	8.2	

[a] Estimated standard deviations: $g_{\|\|}$ and $g_\perp$ ±0.002. $A_{\|\|}$ and $A_\perp$ ±0.5 G. Conditions: acetonitrile solvent, 1.5 M MeIm axial base, frozen glass at −196 °C.

comparison to corresponding substituted species (Figure 8, Tables 6 and 7). CoC6MeHH binds dioxygen approximately 400 times less strongly than its methyl substituted counterpart, CoC6MeMeMe, giving equilibrium constants close to those of CoC4MeMeMe. The dioxygen affinity of CoC8MeHH falls between those of CoC5MeMeMe and CoC6MeMeMe. These dramatic changes can be explained on the basis of the electronic and steric changes accompanying the replacement of the alkyl substituents.

The substantial influence on dioxygen affinity exerted by the electron donating properties of the substitutents has been discussed in much detail.[1b] Both the nature of the substitution and the position at which it occurs are important. Replacement of the methyl group by hydrogen at R^2 in CoC6MeMeMe causes an approximately 10-fold decrease in dioxygen affinity, while the same transformation at R^3 causes a 130-fold decrease. In the present examples, the methyl groups at both the R^3 and R^4 positions are replaced by hydrogen. Not surprisingly the decrease in dioxygen affinity is greater than that observed for CoC6MeHMe. Attributing a lowering of the dioxygen affinity to electronic factors is also consistent with the high Co(III/II) redox potentials of unsubstituted cyclidenes. However, electronic factors are not solely responsible for the low dioxygen affinity of the unsubstituted cyclidenes: (a) While the redox potentials of nickel unsubstituted cyclidenes fall in the range typical of all nickel cyclidene complexes (Table 4), the redox potentials for cobalt unsubstituted cyclidenes seem to be exceptionally high. This is indicative of substantially hindered

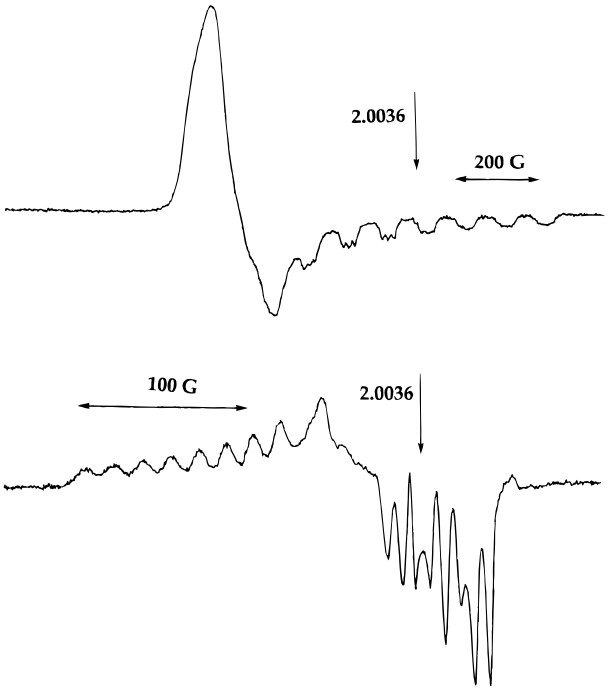

Figure 6. ESR spectra in acetonitrile solution at −196 °C of the square pyramidal cobalt(II) complexes: (a) [Co(C6MeHH[16]cyclidene)MeIm]-$(PF_6)_2$ and (b) [Co(C6MeHH[16]cyclidene)MeIm(O_2)]$(PF_6)_2$.

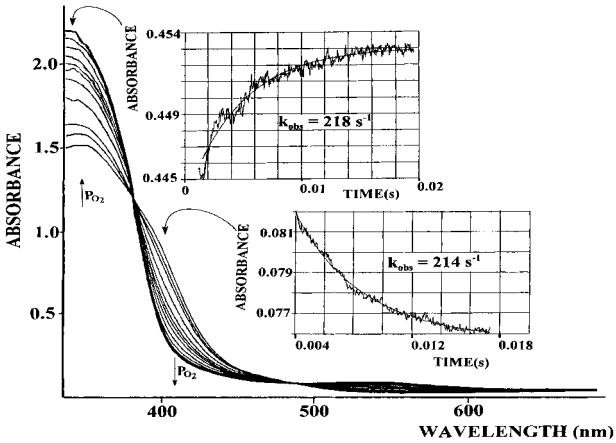

Figure 7. Electronic spectra of 5×10^{-5} M acetonitrile/1.5 M MeIm solution of [Co(C8MeHH[16]cyclidene)]$(PF_6)_2$ at different partial pressures of dioxygen at 0 °C. Partial pressures: ~0; 1.3; 2.6; 6.4; 13; 19; 26; 38; 77; 153; 306; 460; 613; 766 Torr. Inset: Kinetic traces at 410 and 350 nm superimposed with first-order (one-exponential) curve fits obtained in acetone/1.5 M MeIm solution at −75 °C; initial concentration of Co complex 7×10^{-6} M, initial concentration of O_2 2×10^{-5} M.

solvent molecule coordination under the bridge. Since the C6 and C8 bridges in CoCnMeMeMe provide enough space for axial coordination of a sixth ligand, restrictions in axial coordination for CoCnMeHH are clearly connected to the bridge conformation. (b) Changing the bridge length from C6 to C8 for the CoCnMeMeMe cyclidenes results in a 4−5-fold increase in oxygen affinity (entries 5 and 12, Table 7). The same bridge length increase for the CoCnMeHH cyclidenes results in almost 30-fold increase in oxygen affinity (entries 8 and 14, Table 7) indicating more substantial structural changes from the standpoint of accessibility of the sixth site by a ligand.

X-ray crystallographic information clarifies this matter. The folded C6 bridge in CoC6MeMeMe cyclidene has the ability to flip out, away from the cavity, and provide a convenient coordination site for dioxygen binding (Figure 5). The low

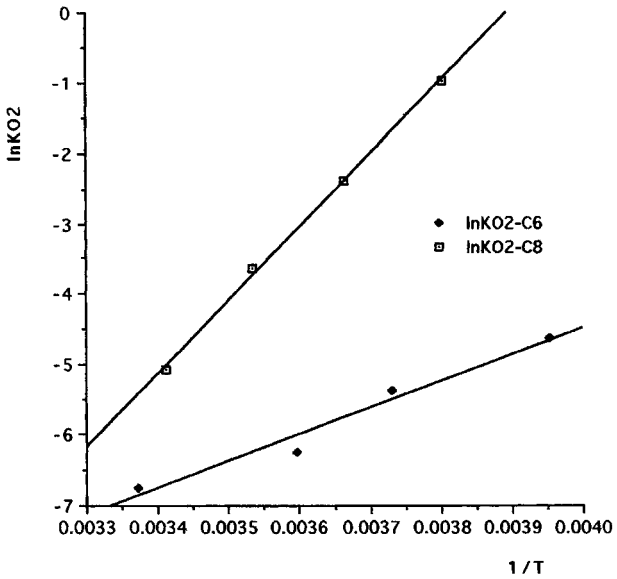

Figure 8. van't Hoff plots for equilibrium constants of dioxygen binding with CoC6MeHH and CoC8MeHH.

Table 6. Dioxygen Affinities for the Unsubstituted Cobalt(II) Cyclidenes at Different Temperatures[a]

$R^1R^2R^3R^4$	K_{O_2} (Torr^{-1}) [(°C)]
C6MeHH	0.0099 [−20.0]; 0.0047 [−5.0]; 0.0020 [5.0]; 0.0012 [23.5]
C8MeHH	0.376 [−10]; 0.092 [0.0]; 0.026 [10]; 0.006 [20]

[a] In acetonitrile/1.5 M methylimidazole.

Table 7. Selected Dioxygen Affinities for the Cobalt(II) Cyclidenes[a]

	$R^1R^2R^3R^4$	K_{O_2} (Torr^{-1})	ΔH,[b] kcal/mol	ΔS,[b] eu	ref
1	C4MeMeMe	0.0020 (−40 °C)			1b
2	C5MeMeMe[b]	0.064	−16.2	−42	1b, 23
3	C5HMeMe	0.0066	−15.4	−44	1b, 23
4	($C_2CMe_2C_2$)MeMeMe	0.027	−9.2[c]	−18[c]	1b, 23
5	C6MeMeMe	1.3	−17.2	−40	1b, 23
6	C6HMeMe	0.14	−17.6	−45	1b, 23
7	C6MeHMe	0.010	−15.0	−41	1b, 23
8	C6MeHH[b]	0.0032	−7.6	−17	this paper
9	C6MePhMe	0.85	−17.8	−42	1b, 23
10	C7MeMeMe	4.5	−18.3	−41	1b, 23
11	C7HMeMe	0.80	−17.3	−41	1b, 23
12	C8MeMeMe	5.92	−17.3	−37	1b
13	C8HMeMe	1.7			1b, 23
14	C8MeHH	0.092	−20.8	−58	this paper

[a] In acetonitrile/1.5 M methylimidazole, 0 °C. [b] Calculated from temperature dependence. In order to get the entropy values in cal/K mol, we assumed the oxygen solubility in acetonitrile to be 8.1 mM (Achord, J. M.; Hussey, C. L. *Anal. Chem.* **1980**, *52*, 601), and the temperature dependence of O_2 solubility was ignored. The entropy values in cal/K Torr which were reported earlier (ref 23) can be obtained from these numbers by subtracting 22.9. [c] Two data points are available.

energy, straight conformation of the bridge in CoC6MeHH is unique and obviously inhibits O_2 binding; no relatively open low energy conformation can compete. The straight conformation of the bridge in CoC6MeHH must either substantially restrict the approach of dioxygen to the metal center or lead to unfavorable geometry within the dioxygen adduct itself. This is an issue that is addressed in the studies on rates of binding and dissociation.

The changes in bridge conformation in going from CoC6MeMeMe to CoC6MeHH are traceable to the elimination of vicinal R^2R^3 methyl−methyl repulsions, and this observation is readily extended to other cases. Despite the electron-withdrawing effect of phenyl groups, CoC6MePhMe binds oxygen 85 times more strongly than the complex with hydrogens at the corresponding R^3 positions CoC6MeHMe. R^2R^3 vicinal repulsion in the phenyl substituted complex forces the bridge to fold, opening the cavity to O_2, whereas CoC6MeHMe, with no R^2R^3 vicinal repulsion probably, has a confining straight bridge like CoC6MeHH. The decreases in the ratios of the dioxygen affinities for CoCnMeHMe compared to CoCnMeMeMe is approximately 10-, 9-, 6-, and 3.5-fold, respectively, for $n = 5$, 6, 7, and 8, respectively. For the longer bridges, the response to the removal of vicinal repulsion becomes smaller, because completely straight conformations are no longer achievable.

For most of the previously studied cyclidenes, variations in ΔH and ΔS are relatively small (Table 7, Figure 8); ΔH ranging from −15 to −18 kcal/mol, and ΔS varying between −37 and −44 e.u. However, for the unsubstituted cyclidenes, oxygenation of CoC8MeHH ($\Delta H = -20.9$ kcal/mol) is distinctly more exothermic than the average for cobalt cyclidene complexes (about −17 kcal/mol); while the corresponding value of ΔH for CoC6MeHH is unusually small (−7.6 kcal/mol). The latter value is comparable only to the value for Co($C_2CMe_2C_2$)-MeMeMe cyclidene, a material bearing a highly hindered, moderately short C5 bridge (ca. −9 kcal/mol).[23] These results suggest that the bridges in both CoC6MeHH and Co$C_2CMe_2C_2$-MeMeMe restrict access to the cobalt atom and weaken Co-dioxygen interaction.

Kinetics of Dioxygen Binding. The equilibrium constant for dioxygen binding with cobalt complexes is determined by the rate constants of O_2 binding and dissociation:

$$\mathrm{Co(L)(B)} + \mathrm{O_2} \underset{k_{off}}{\overset{k_{on}}{\rightleftarrows}} \mathrm{Co(L)(B)(O_2)} \quad K_{O_2} = k_{on}/k_{off} \qquad (1)$$

Historically, steric hindrance deriving from the superstructure of a macrocyclic ligand has been found to affect k_{on}, causing decreases in binding rates as the cavity shrinks.[3c,4d] This effect, traceable to the entropy of activation, is attributed to limited access of the dioxygen molecule to the cobalt(II) ion: only a restricted fraction of the possible O_2 and complex orientations permit Co−O_2 interaction. In contrast, electronic effects (e.g., changing the axial base B) lead to significant changes in the dissociation rates (the weaker the Co−O_2 bond, the faster the dissociation).[3c,5d] These trends were also observed for CoCn-MeMeMe cyclidenes ($n = 4-6$).[24]

The kinetics of oxygenation of unsubstituted cyclidenes were studied at low temperature (−75 °C) by a cryogenic stopped-flow technique with spectrophotometric monitoring of concentration changes, because (1) at low temperatures the process is slow enough to permit the precise recording of kinetic traces and (2) equilibrium (1) is shifted toward dioxygen adduct formation at low temperatures, enhancing precision. Further, the reverse reaction is suppressed, and a simple second-order rate law applies:

$$v = k[\mathrm{Co(L)(B)}][\mathrm{O_2}] \qquad (2)$$

This simplification of the rate law was very important in our case, because variations in the concentrations of the reagents were confined by rapid rates and the sensitivity of the instrumentation. Unfortunately, this strategy prevented direct measurement of the rates of dioxygen dissociation.

(23) Busch, D. H.; Jackson, P. J.; Kojima, M.; Chmielewski, P.; Matsumoto, N.; Stevens, J. C.; Wu, W.; Nosco, D.; Herron, N.; Ye, N.; Warburton, P. R.; Masarwa, M.; Stephenson, N. A.; Christoph, G.; Alcock, N. W. *Inorg. Chem.* **1994**, *33*, 910.

(24) Rybak-Akimova, E. V.; Masarwa, M.; Marek, K.; Warburton, P. R.; Busch, D. H. *Chem. Commun.* **1996**, 1451.

Table 8. Kinetic Parameters for Dioxygen Binding to Cobalt(II) Cyclidenes[a]

	compd	k_{on}, M^{-1} s^{-1} (−75 °C)	$\Delta H_{on}^{\ddagger}$, kcal/mol	ref
1	CoC4MeMeMe	5×10^3	2.2	calcd from 25
2	CoC5MeMeMe	2×10^5	0.7	calcd from 25
3	CoC6MeMeMe	$(5 \pm 1) \times 10^6$	4[b]	25, this paper
4	CoC6MeHH	$(4 \pm 1) \times 10^6$	3[b]	this paper
5	CoC8MeMeMe	$(2 \pm 0.5) \times 10^7$	4[c]	this paper
6	CoC8MeHH	$(2 \pm 0.5) \times 10^7$	4[d]	this paper

[a] In acetone−1.5 M 1-methylimidazole, at −75 °C. [b] ±1 kcal/mol. [c] Estimated from three data points. [d] Estimated from two data points.

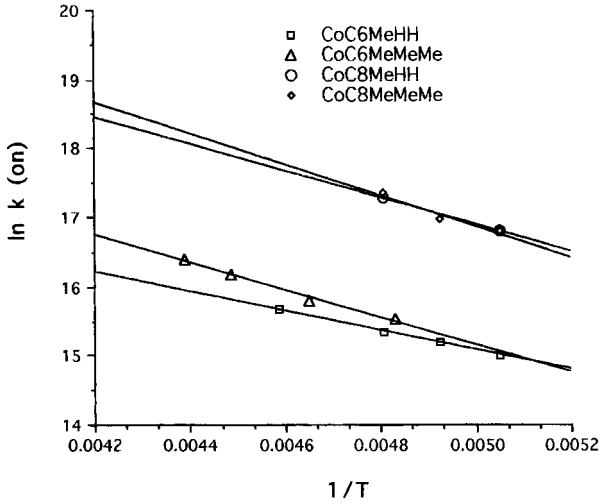

Figure 9. Temperature dependence of the second-order rate constants for the oxygenation of cobalt(II) cyclidenes (1.5 M 1-MeIm/acetone).

Absorbance changes upon mixing in the stopped flow experiments correspond very well to those observed during spectrophotometric titrations (Figure 7), and the rate constants determined at different wave lengths are identical. In acetone, rates do not depend on the axial base concentration over the range studied (0.5−1.5 M 1-methylimidazole), but they do depend on the concentrations of cobalt(II) complex and dioxygen (Table 8).[25] For the two complexes having C6 bridges, significant variations of reagent concentrations (about 1 order of magnitude) and pseudo-first-order conditions were accessible. For the C8 bridged complexes,[26] the reactions are faster, and reasonable kinetic traces could be determined only for a relatively narrow range of reagent concentrations, limiting the second-order rate constants to uncertainties of about 50%.

The activation energies for oxygenation reactions were estimated from Arrhenius plots (Figure 9). Because of high reaction rates, measurements were limited to the temperature range from −75 to −50 °C for C6 bridged compounds and from −75 to −65 °C for C8 bridged compounds. While it is obvious that such temperature ranges are not adequate for precise determination of activation enthalpies and entropies, these limited data clearly show that the activation energies are relatively small and very similar for all of the complexes under investigation (Figure 9). Because, this general result requires the oxygenation rates for CoC6MeMeMe, CoC8MeMeMe, CoC6MeHH, and CoC8MeHH to display almost parallel temperature dependencies, we can justify the extrapolation of oxygenation rates beyond the very low temperature range for the purpose of making comparisons.

The most general conclusions from these rate studies are very clear. Despite substantial differences in dioxygen affinities between unsubstituted cyclidenes and their methyl-substituted analogs (see above), the rates of dioxygen binding of CoCnMeMeMe and CoCnMeHH are essentially identical (for the same bridge length *n*). This indicates that, at the transition state for O_2 binding, there is no substantial difference between methyl-substituted and unsubstituted cyclidenes. Further, the very small activation enthalpy suggests that the transition state occurs early in the Co−O bond-forming process, a scenario consistent with the identity of the rates for the two rather different cobalt compounds.

In contrast, it was shown above that the dramatic difference in dioxygen affinity between CoC6MeMeMe and CoC6MeHH can be explained by a combination of steric and electronic factors. Now, the kinetic data tell us that the nature of the steric factor is different from that usually observed (usually, k_{on} is affected).[27] From the equilibrium constants and the rate constants for binding, we can conclude that the rate constants for dissociation must account for the differences in dioxygen affinities. Clearly, the difference in the bridge conformation for CoC6MeHH accelerates O_2 departure (when compared to CoC6MeMeMe), indicating that the Co−O linkage is weakened.

For both the unsubstituted and methyl-substituted complexes, the C8 bridge permits dioxygen binding that is approximately five times faster than that for the C6 bridged derivative. A similar rate/bridge length trend has been reported for a series of C4−C6 methyl-substituted cobalt cyclidenes.[24] The increase in rate constants for O_2 binding with increasing cavity size is attributable to the activation entropy and is associated with entry of the dioxygen into the lacuna. The difference in dioxygen affinities between CoC6MeMeMe and CoC8MeMeMe (five times) is completely assignable to different binding rates, while differences in both binding and dissociation rates contribute to the difference in O_2 affinities between CoC6MeHH and CoC8MeHH (30 times).

Autoxidation. Previous studies on the kinetics and mechanism of autoxidation of cobalt(II) cyclidene−dioxygen adduct[6,28] revealed a conjugate base mechanism in which deprotonation may occur either in the rate determining step or in a preequilibrium step. In previous studies, substitution for relatively acidic protons at the R^2 and R^3 positions had given orders or magnitude decreases in rates of autoxidation, but the same conjugate mechanism persisted, albeit at much retarded rates. In view of the well demonstrated role of a methyl group at the R^3 as the site for acceleration of autoxidation due to deprotonation, suspicion fell on the ubiquitous R^4 methyl groups. The synthesis of the so-called unsubstituted cyclidenes followed and is reported here. Preliminary rate data on the autoxidation

$$CoLH(O_2)^{2+} + B \overset{\text{slow}}{\rightleftarrows} CoL(O_2)^{2+} + BH \overset{\text{fast}}{\rightleftarrows} \text{products} \quad (3)$$

of these new compounds completes the work presented here. Since the suspected acidic methyl groups R^4 have been eliminated from the structures of the unsubstituted cyclidenes, increased stability toward autoxidation is expected. The results of the most preliminary of experiments showed that this was indeed the case since the autoxidation reactions are very slow under conditions used in previous studies of the many R^4 =

(25) O_2 solubility in acetone at 25 °C (temperature at which dioxygen solutions were prepared for our kinetic measurements) is reported to be 11.5 mM (Linke, W. F. *Solubilities of Inorganic and Metal-Organic Compounds*; American Chemical Society: Washington, DC, 1965), or 11.0 mM (Achord, J. M.; Hussey, C. L. *Anal. Chem.* **1980**, *52*, 601). An average value of 11.2 mM has been used in our calculations of O_2 concentration.

(26) CoC8MeMeMecyclidene (hexafluorophosphate salt) was synthesized according to ref 15b.

(27) Distal side steric effects usually derive from accessibility of the metal ion and appear in k_{on} (refs 3c and 4d).

(28) Chia, P. S. K.; Masarwa, M.; Warburton, P. R.; Wu, W.; Kojima, M.; Nosco, D.; Alcock, N. W.; Busch, D. H. *Inorg Chem.* **1993**, *32*, 2736.

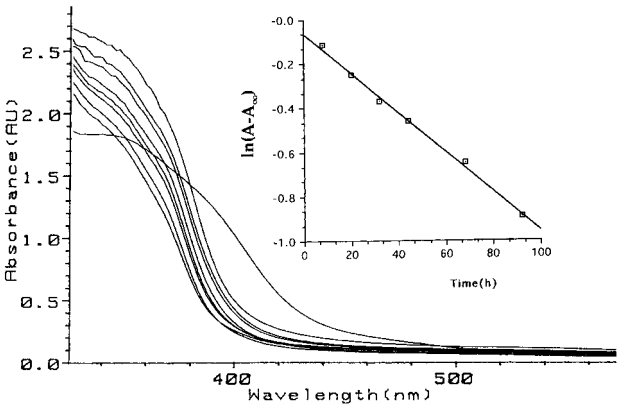

Figure 10. Absorbance changes in the course of CoC8MeHH autoxidation (5×10^{-5} M solution of complex in 1.5 M 1-MeIm/acetonitrile, 760 Torr O_2). Reactions run at 30 °C, spectra recorded at 20 °C for nonoxygenated complex and 0; 4; 8; 20; 32; 44; and 72 h after oxygenation. Inset: linear first-order kinetic curve (measured at 348 nm).

Table 9. Observed Pseudo-First-Order Rate Constants for the Autoxidation of Co(II) Cyclidene Complexes in 1.5 M 1-Methylimidazole−Acetonitrile, 30 °C, 760 Torr of Dioxygen

	complex	k_{obs}, s^{-1}	ref
1	CoC3MeMeMe[16]$^{2+}$	2.0×10^{-5}	6
2	CoC4MeMeMe[16]$^{2+}$	2.0×10^{-5}	6
3	CoC5MeMeMe[16]$^{2+}$	2.0×10^{-4}	6
4	CoC6MeMeMe[16]$^{2+}$	4.0×10^{-4}	6
5	CoC7MeMeMe[16]$^{2+}$	1.0×10^{-3}	6
6	CoC8MeMeMe[16]$^{2+}$	8.0×10^{-4}	6
7	CoC8HMeMe[16]$^{2+}$	1.0×10^{-2}	6
8	CoC6MePhMe[16]$^{2+}$	2.0×10^{-5}	6
9	CoC6MeHH[16]$^{2+}$	4.0×10^{-6}	this paper
10	CoC8MeHH[16]$^{2+}$	2.5×10^{-6}	this paper

methyl complexes; this required special techniques for the determinations reported here (see Experimental Section; Figure 10). The data in Table 9 indicates a substantial decrease (5−8 times) in autoxidation rates for unsubstituted cyclidenes when compared with the most stable cobalt(II) cyclidenes previously investigated, confirming the prediction. The high redox potentials of the unsubstituted cyclidenes may also contribute to their slow rates of autoxidation. Detailed investigation of the kinetics and mechanism of autoxidation of the unsubstituted cyclidenes is the subject of further research. The simple measurements reported here merely confirm the hypothesis that removal of the suspected R^4 groups does indeed lead to dioxygen carriers that autoxidize more slowly. Clearly that is true. It will be of interest to learn if the same mechanism still persists, perhaps involving the methylene protons of the saturated chelate rings, or if some entirely new autoxidation mechanism has appeared.

Conclusions

The family of cyclidene ligands continues to be remarkably flexible and appropriate for the process of iterative molecular design through which so-called ideal dioxygen carrier structures are being approached incrementally. A very slow rate of autoxidation, or none at all, is a requisite property of the ideal dioxygen carrier. Previously, mechanistic studies have shown that ionizable protons support a conjugate base mechanism for the autoxidation of the cobalt(II) cyclidene dioxygen adducts, and with the completion of the present work, all substituents capable of contributing to that process have now been eliminated. The results have been striking; the rate of autoxidation has been retarded by some 4 orders of magnitude by controlling that structural weakness alone. Unfortunately, the complexes still undergo autoxidation, albeit, at the slowest rate so far observed for compounds of this class. If this slow autoxidation rate is associated with the familar conjugate base mechanism, then the likely source of deprotonation involves the trimethylene groups of the saturated six-membered chelate rings. Improved molecular design will obviate this possibility in the future.

Removal of the methyl substituents from the unsaturated portion of the parent cyclidene ring produced an unexpected decrease in O_2 affinity, especially in the case of the hexamethylene bridged complex. While this is attributable in part to decreased electron density at the metal atom, a profound change in the conformation of the bridging hexamethylene chain is mainly responsible. Exploring this phenomenon has led to increased understanding of the manner in which the bridging group controls O_2 affinity and an exceptionally clear example of a steric effect in which the weakening of the Co−O bond causes an increase in the rate of dissociation of O_2. This further increases the number of structural relationships available to fine tune dioxygen affinity.

Acknowledgment. This material is based upon work supported by the NSF under Grants numbered OSR-9255223 and CHE-9118455 and matching support from the state of Kansas. The collaboration between The University of Kansas and The University of Warwick has been supported by a NATO travel grant. We wish to thank Dr. Todd Williams, Mr. Bob Drake, and Ms. Homigol Biesiada of the University of Kansas for the efforts in acquiring mass spectra. The authors also greatly appreciate the contributions to the acquisition of 2-D NMR data by Dr. Martha Morton. Dr. Tho Nguyen of the University of Kansas supplied elemental analysis. These contributions are deeply appreciated.

Supporting Information Available: Tables listing anisotropic thermal parameters, H-atom coordinates, full bond lengths and angles, and atomic coordinates (6 pages). See any current masthead page for ordering and Internet access instructions.

JA9624477